First plasma and tissue pharmacokinetic study of the YSNSG cyclopeptide, a new integrin antagonist, using microdialysis

Florian Slimano, Zoubir Djerada, Salim Bouchène, Laurence van Gulick, Sylvie Brassart-Pasco, Sylvain Dukic

First plasma and tissue pharmacokinetic study of the YSNSG cyclopeptide, a new integrin antagonist, using microdialysis

Florian Slimano[a,b,*,1], Zoubir Djerada[c,1], Salim Bouchene[c], Laurence Van Gulick[a], Sylvie Brassart-Pasco[a], Sylvain Dukic[a,b]

[a]MEDyC Research Unit, UMR CNRS/URCA n°7369, SFR CAP-Santé, Reims University; Faculty of Pharmacy, 51, rue Cognacq-Jay; 51100 Reims

[b]Department of Pharmacy, University Hospital Reims, Avenue du General Koenig, 51100 Reims

[c]Department of Pharmacology and Toxicology, EA3801, SFR CAP-Santé, University Hospital Reims; Faculty of Medicine, 51, rue Cognacq-Jay; 51100 Reims

* *Corresponding author:*
Florian Slimano
Faculty of Pharmacy
Reims University
51, rue Cognacq-Jay, 51100 Reims
florian.slimano@univ-reims.fr
Tel: (+33)3.26.91.80.81

Abstract

The YSNSG peptide is a synthetic peptide targeting $\alpha_v\beta_3$ integrin. This peptide exhibits promising activity *in vitro* and *in vivo* against melanoma. To determine pharmacokinetic parameters and predictive active doses in the central nervous system (CNS) and subcutaneous tissue (SC), we conducted microdialysis coupled with pharmacokinetic modeling and Monte Carlo simulation. After a recovery period of surgical procedures, a microdialysis probe was inserted in the caudate and in subcutaneous tissue. Plasma samples and dialysates collected 5 hours after YSNSG intravenous administration (10 mg/kg) were analyzed by UPLC-MS/MS. A nonlinear mixed-effect modeling approach implemented in Monolix® 2016R1 was performed. Model selection and evaluation were based on the usual diagnostic plot, precision and information criteria. The primary plasma and tissue pharmacokinetic parameters were comparable with those of other integrin antagonists, such as cilengitide or ATN-161. Tissue/plasma and brain/plasma area under the curve (AUC) ratio were 66.2±21.6% and 3.6±4.7%, respectively. Two models of 2-compartments with an additional microdialysis compartment, parameterized as rate constants (k for elimination, k12/k21 and k13/k31 for distribution) and volumes (central V1 and peripheral microdialysis compartment V3) with zero-order input were selected to describe the dialysate concentrations in CNS and SC. The inter-individual variability (IIV) was described by exponential terms, and residual variability was described by a combined additive and proportional error model. Individual AUC (plasma and tissues) values were derived for each animal using the Empirical-Bayes-Estimates of the individual parameters. The regimens needed to achieve an *in vitro* predetermined target concentration in tissues were studied by Monte Carlo simulations using Monolix® 2016R1. YSNSG pharmacokinetic parameters show promising results in terms of subcutaneous disposition. Further investigations into such processes as encapsulation and intratumoral disposition are currently being conducted.

1. Introduction

Currently, studies on the structure of the extracellular matrix (ECM) have been demonstrated to be fundamentally important to understand carcinogenesis mechanisms. Interactions between tumor cells and the endothelial wall via the ECM are dependent on cell adhesion molecules (CAM) (Hynes, 2002). Among these, integrins, heterodimeric transmembrane glycoproteins, play a fundamental role as cellular receptors in the carcinogenesis process (Francavilla et al., 2009; Shattil et al., 2010). Although many subfamilies of integrins exist with different subunits, the "alpha v beta 3" ($\alpha_v\beta_3$) vascular integrin was reported to play an important role in cancer development, including angiogenesis and tumor growth (Brooks et al., 1994; Ley et al., 2016; Soldi et al., 1999). As such, deregulation of its expression and activity has been linked to cancer progression similar to that in melanoma (Danen et al., 1995; Edward, 1995; Kuphal et al., 2005). Researchers have found that a motif of only three amino acids (Arginine-Glycine-Aspartate, “RGD”) can bind strongly to $\alpha_v\beta_3$ (Felding-Habermann and Cheresh, 1993; Pierschbacher and Ruoslahti, 1984), although the non-RGD motif can also interact with this integrin (Ley et al., 2016). Cilengitide, a cyclic pentapeptide with an RGD motif, shows promising outcomes in glioblastoma despite its failure to improve overall survival in a phase 3 trial (Stupp et al., 2014). However, cilengitide is still being studied in metastatic melanoma, recurrent or metastatic head and neck tumors and non-small cell lung cancer clinical trials with uncertain results (Kim et al., 2012; Vansteenkiste et al., 2015; Vermorken et al., 2014). By contrast, ATN-161, a linear non-RGD-based peptide motif that binds $\alpha_5\beta_1$ and $\alpha_v\beta_3$ integrins has shown promising activity *in vivo* by inhibiting tumor growth and metastasis in preclinical and phase I clinical studies (Cianfrocca et al., 2006; Khalili et al., 2006; Livant et al., 2000; Stoeltzing et al., 2003). Our research group isolated a (linear) original peptide from collagen IV and showed anticancer activity in melanoma models both in

vitro and in vivo, especially in terms of tumor growth inhibition (Thevenard et al., 2006). Other similar studies based on human gastric carcinoma and human glioma cell lines have shown similar in vitro and in vivo results in terms of tumor growth inhibition, apoptosis induction, increased expression of Fas, FasL, caspase-3 and decreased expression of Vascular Endothelial Growth Factor (VEGF), basic Fibroblast Growth Factor (bFGF) and antiangiogenesis (He et al., 2010; Li et al., 2009; Ye et al., 2013). After reduction to an active sequence of four amino acids and cyclization with glycine [Tyr-Ser-Asn-Ser-Gly], the peptide [YSNSG] showed significantly inhibition of tumor growth in vivo after intraperitoneal administration in mice with a melanoma tumor (Thevenard et al., 2006). This synthetic cyclopeptide also exhibits anti-angiogenic activity as reflected by a reduced number of intratumoral microvessels (Thevenard et al., 2010).

No pharmacokinetic study has been performed to date. In this work, we investigated the first pharmacokinetic study of the main plasmatic pharmacokinetic parameters. In coherence with the anticancer potential of YSNSG in melanoma models, we also investigated the disposition of YSNSG in two tissues: subcutaneous tissue, which corresponds to the primary site of cutaneous melanoma, and cerebral tissue, which corresponds to the frequent metastatic localization of melanoma. Thereafter, we utilized a pharmacokinetic modeling approach and Monte Carlo simulation to predict and validate a pharmacokinetic model. From this model, we performed certain simulations of doses and constant rate of infusion to achieve pharmacologically active concentrations.

2. Materials and Methods

2.1. Chemicals

YSNSG (powder) was obtained from Ansynth (Le Roosendaal, the Netherlands). Isoflurane (ISOFLO®) was from Centravet (Nancy, France). Sodium chloride, potassium chloride,

magnesium sulfate, sodium bicarbonate, glucose, sucrose, and calcium chloride were from Cooper (Melun, France). Saline solution (0.9%) VERSOL® was from Aguettant (Lyon, France). For brain microdialysis, artificial cerebrospinal fluid (aCSF) was prepared containing the following as previously described (Cold Spring Harbor Protocols, 2007): 124 mM NaCl, 2.5 mM KCl, 2 mM $MgSO_4$, 1.25 mM K_2HPO_4, 26 mM $NaHCO_3$, 10 mM $C_6H_{12}O_6$, 4 mM $C_{12}H_{22}O_{11}$, 2.5 mM $CaCl_2$, adjusted to pH 7.4.

2.2. Animals

The study protocol was approved by the Ethics Committee of Animal Experimentation of Reims University (the *comité d'éthique en expérimentation animale de Reims Champagne-Ardenne*; C2EA-56). Male Wistar rats (225-250 g in weight; Charles River, l'Arbesle, France) were penned in a controlled environment (temperature: 21 ± 2 °C; relative humidity: 65 ± 15%; alternating natural light/dark cycles). The animals were fed a standardized diet (UAR, Villemoisson on barley, France), and tap water was provided *ad libitum*.

2.3. Surgery

Twenty-four healthy adult male Wistar rats were prepared seven days before pharmacokinetic experimentation. Surgery preparation involved the implantation of a microdialysis guide (CMA/11; Phymep, Paris, France) into the brain. Implantation was performed under anesthesia (isoflurane 3-5%) with an evaporator (Isotec 4: Ohmeda, Maurepas, France). The animal's head was then fixed to a stereotaxic apparatus (Model Stoelting 51600; Phymep, Paris, France), and a drilled hole was made in the skull bone to the right caudate nucleus (1 mm anterior, 4 mm lateral, 4 mm ventral, relative to the Bregma in the skull flat block). The microdialysis guides were secured to the skull with 3 anchor screws (Carnégie; Phymep, Paris, France) and dental cement (Autenal Dental, Harrow, England). Overall, the skull was drilled 4 times with a dental drill (Anthogyr, Sallanches, France). Between the surgery and

experiments, the animals were kept individually in cages for 7 days to recover from the surgical procedures.

2.4 YSNSG dilution and administration

YSNSG reconstitution for intravenous administration was performed by diluting in saline to obtain a concentration of approximately 2 mg/mL (depending on the dose for 10 mg/kg). YSNSG was administered via the penis vein at 1 mL/min.

2.5. Pharmacokinetic experimentation

All animals (n = 24), first anesthetized with isoflurane (1.5-5%), underwent the intravenous administration (i.v.) of YSNSG at 10 mg/kg. Anesthesia was administered for 300 min after the installation of a tracheal cannula (Harvard Apparatus, Les Ulis, France) connected to a respirator (Small Animal Ventilator, Harvard) during which the rat was kept at 37 °C with a heater bulb and a heating mat. The temperature was monitored through a rectal thermometer (Harvard Apparatus, Les Ulis, France), and the breathing frequency was adapted to each animal depending on its weight with an abacus (80/min), and the current volume delivered to the animal was continuously monitored by measuring tele expiratory CO_2 using a CO_2 analyzer (Engström eliza, Paris, France). The values were kept between 4.2 and 4.7%. An adapted microdialysis probe (CMA/11) was placed in the brain, and then a second one was placed subcutaneously (CMA/20) on the posterior surface on the left thigh with a 30-minute waiting period before administration. The probes were connected to a pump infusing artificial CSF and physiological saline to the brain and skin (perfusate), respectively, with a throughput of 1 µL/min. Blood samples were taken at the following time intervals: 2.5, 5, 10, 20, 40, 60, 90, 120, 180, 240, and 300 minutes. They were then temporarily stored in heparin (0.2 IU)-coated Eppendorf cups before being centrifuged for 10 min at 4000 rpm. The plasma was then pipetted into clean Eppendorf cups and was stored at -20 °C for subsequent analysis.

Dialysates were collected (every 30 min) in vial cups (100 µL) using a refrigerated fraction collector (820 Microsampler, UNIVENTOR) and were stored at -20°C for subsequent analysis. At the end of the experiments, the animals were sacrificed.

2.6. Recovery of microdialysis probes

In vivo microdialysis probe recoveries of YSNSG were determined based on reverse dialysis (Ståhle et al., 1991). The same surgery was performed on four Wistar rats. Seven days after the establishment of a microdialysis cannula, the animals were anesthetized with isoflurane. A microdialysis probe implanted in the brain parenchyma or subcutaneously was infused at a rate of 1 µL/min with a solution containing YSNSG (at a controlled concentration of 500 ng/mL in CSF or normal saline, respectively). Thirty-minute-interval sample dialysates were collected between 30 and 300 min. *In vivo* recovery is defined as the ratio of the concentration difference between the dialysate (C_{out}) and perfusion fluid (C_{in}) over the concentration in the perfusion fluid (Eq. (1)) (Scheller and Kolb, 1991).

$$\textit{In vivo}\ \text{recovery} = \frac{Cin - Cout}{Cin} \quad (1)$$

2.8. Plasma protein binding

To determine the plasma protein binding (PPB) of YSNSG, plasma samples at different time points were pooled to span the entire concentration range. Plasma protein binding was determined using the Centrifree ultrafiltration device with a YM-T Ultracel® membrane (Dutscher SA, Brumath, France). All procedures were performed according to the user's manual. The ultrafiltrate was diluted 10 times with saline before the analysis.

2.9. Sample pre-treatment and analysis

YSNSG concentrations were determined by UPLC-MS/MS (Djerada et al., 2013) after a 1/1000 dilution (with water + 0.1 % (V/V) formic acid) of plasma or microdialysates. All compounds (YSNSG and MRFA as the internal standard) were eluted within a 3.5-min run time using a programmed mobile-phase gradient of water/0.1 % (V/V) formic acid and acetonitrile/0.1 % (V/V) at a flow rate of 0.8 mL/min. Chromatographic separation was achieved using a Waters Acquity HSS T3 (2.1 × 50 mm) UPLC column (Waters Corp., Milford, MA, USA), maintained at 50 °C. Mass spectrometry detection was performed using a Xevo TQ mass spectrometer (Waters Corp., Milford, MA, USA) after electro-spray ionization in the positive ion mode with the following parameters: capillary voltage of 1.0 kV, desolvatation temperature at 450 °C, gas flow desolvatation at 850 L/h and gas flow cone at 50 L/h. Dry nitrogen (≥99.9%) was used as the desolvatation and nebulization gas, and argon (>99.999%) was used as the collision gas (Air Liquid®, Paris, France). The molecules were used as parent ions for the MS/MS experiment, and the suitable product ions (daughters) were selected: YSNSG 509.30 → 136.10 with a cone voltage = 30 V and energy collision = 30 eV; MRFA 524.40 → 104.10 with a cone voltage = 50 V and collision energy = 30 eV. The system control and data acquisition were performed using MassLynx® software (version 4.1; Waters Corp., Milford, MA, USA). The lower limit of quantification for YSNSG was fixed to 1 ng/mL with a coefficient of variation below 10%. The intra-assay precision and accuracy averaged 5.0% and 5.0%, respectively. The inter-assay precision and accuracy averaged 11.0% and 11.0 %, respectively, which is in line with FDA analytical recommendations.

2.10. Pharmacokinetic analysis

2.10.1 Non-Compartmental analysis

For the non-compartmental analysis, the pharmacokinetic parameters of YSNSG were determined for each animal by linear and nonlinear regression, considering the profiles of

peptide concentrations in plasma using Prism® software (version 6.0; GraphPad Software, San Diego, California, USA) and MicroPharm-K (MicroPharm®, West Wales, UK). The choice of model describing the evolution of the concentration profiles of YSNSG was based on comparing the values of the Akaike information criterion (AIC). The values of the concentrations determined in the extracellular fluid peptide were corrected by returns or performance *in vivo*. The median value of each interval was selected as the sampling time for each concentration measured. The exposure of the caudate nucleus to YSNSG was determined by the ratio of the areas under the curve in the extracellular fluid (ECF) in the brain and plasma (AUC_{ECF} / AUC_{plasma}). This ratio estimated the rate of passage through the area of interest of YSNSG.

2.10.2 Population Pharmacokinetic Modeling

A population approach, with the nonlinear mixed-effect modeling implemented in Monolix (version 2016R1), was used to study the pharmacokinetic profile of YSNSG. The parameters were estimated by computing the maximum likelihood estimator without any approximation of the model, using the stochastic approximation expectation maximization (SAEM) algorithm combined with an MCMC (Markov Chain Monte Carlo: 5 for the number of chain) procedure (Djerada et al., 2014). All runs were carried out more than six times to ensure that the estimated parameters and likelihood remained stable. Using the MLXTRAN language included in Monolix (version 2016R1), one, two and three mammillary compartment models, with zero- or first-order input, a lag time, and first-order elimination were tested to describe the observed YSNSG concentrations in plasma and tissues (CNS and SC). Separate structural models of YSNSG concentrations were described using compartmental pharmacokinetic modeling (Fig. 1). All individual parameters were defined as log-normally distributed. Several error models (constant, proportional, additive or mixed, exponential and logit error model) were studied to describe the residual variability (ε). The between-subject variability (BSV) of

the pharmacokinetic parameters was described using an exponential model as follows: $\theta i = \theta TV \times \exp(\eta i)$, where θi is the estimated individual parameter, θTV the typical value of the parameter and ηi the random effect for the ith animal. The values of ηi were assumed to be normally distributed, with mean 0 and variance ($\omega 2$), which were parameterized as a diagonal matrix. The model best describing individual data was evaluated based on the usual diagnostic plot, precision and information criteria. The likelihood ratio test (LRT), including the −2 log-likelihood, AIC and Bayesian information criterion (BIC), was used to test different hypotheses regarding the final model: residual variability model (proportional versus proportional plus additive error model) and the structure of the variance-covariance matrix for the interindividual variability parameters. In addition, eta (η) shrinkage was quantified as recently described (Lavielle and Ribba, 2016).

To evaluate the accuracy and robustness of the model appropriateness across time, prediction-corrected visual checks with 1000 simulated data sets were used. The observed concentrations were overlaid on the prediction intervals and compared visually. The normal distribution of normalized prediction distribution errors (NPDE) metrics was tested. As for NPDE, population or individual weighted residuals (PWRES or IWRES) vs. time and PWRES or IWRES vs. predictions should be centered on zero, without systematic bias. Individual pharmacokinetic parameters were derived for each animal using the Empirical-Bayes-Estimates (EBE) of the individual parameters determined by the final model.

3. Results

All results are presented as average values ± standard error of the mean, unless stated otherwise.

3.1. In vivo recovery and plasma protein binding

The performance rates of the microdialysis probes of YSNSG in rats (n=3) using the reverse dialysis method were 36.18 ± 4.9% and 53.4 ± 9.15% in the brain and subdermal tissue, respectively. Both values were used to determine the true values of the tissue concentrations of YSNSG. All values shown in the *Results* were corrected. Plasma protein binding (PPB) was determined at 5.4±2.5% and, similarly, plasma values were corrected accordingly.

3.2 YSNSG pharmacokinetic with non-compartmental analysis

The main plasma and tissue pharmacokinetic parameters determined using the non-compartmental approach are shown in Table 1. The concentration-time profile of YSNSG in plasma showed a bicompartimental decrease with a volume of distribution of 433.7 ± 272.2 mL, an elimination half-life of 2.56 ± 1.52 h and a total clearance of 10.7 ± 6.3 mL/min/kg. The area under the curve (AUC) was 1473.19 ± 1054.99 µg.min/mL. The evolution of subcutaneous pharmacokinetic parameters showed a T_{max} between 0 and 30 min with a C_{max} of 8.57 ± 2.13 µg/mL. The $AUC_{ECF(SC)}/AUC_{plasma}$ ratio was 66.2 ± 21.6%. The evolution of the cerebral concentration showed a T_{max} between 60 and 90 min with a C_{max} of 183 ± 200.4 ng/mL. The $AUC_{ECF(CB)}/AUC_{Plasma}$ ratio was 3.6 ± 4.7 %.

3.3. YSNSG pharmacokinetic models

Two compartments with an additional microdialysis compartment, parameterized at constant rates (elimination k and distribution k12/k21, k13/31) and volumes (central V1 and peripheral microdialysis compartment V3), with zero-order input, was selected to describe the dialysate concentrations in CNS and SC. The between-subject variability (BSV) was described by exponential terms, and the residual variability was described by a combined additive and proportional error model. Table 2 summarizes the results of the two pharmacokinetic models (plasma & SC, plasma & CNS). For the plasma and SC models, the coefficients of correlation between the observed and predicted concentrations (derived from EBE) of YSNSG in the

plasma model were r = 0.986 ($p < 0.0001$, Spearman test, Fig. 2A) and r = 0.894 ($p < 0.0001$, Spearman test, Fig. 2B respectively). For the plasma and CNS models, the coefficients of correlation between the observed and predicted concentrations (derived from EBE) of YSNSG in plasma model were r = 0.974 ($p < 0.0001$, Spearman test, Fig. 3A) and r = 0.711 ($p < 0.0001$, Spearman test, Fig. 3B). All of the parameters were reasonably estimated given their relative standard error (RSE%) and shrinkage values. The highest shrinkage value was for V2 (63% and 62% for subcutaneous and cerebral tissue, respectively), all other shrinkage values are within 26%.

3.4. Evaluation and validation of pharmacokinetic models

The mean and median of the normalized prediction distribution error (NPDE) metrics for YSNSG in the plasma of the plasma and SC models (Fig. 4A to 4D) were not significantly different from 0 ($p = 0.35$, one sample t test; $p = 0.10$, Wilcoxon signed-rank test), and their distributions were not different from a normal distribution ($p = 0.066$, Kolmogorov-Smirnov test of normality). The mean and median of the normalized prediction distribution error (NPDE) metrics for YSNSG in the SC of plasma and SC model (Fig. 4E to 4H) were not significantly different from 0 ($p = 0.36$, One sample t test; $p = 0.09$, Wilcoxon signed-rank test), and their distributions were not different from a normal distribution ($p = 0.067$, Kolmogorov-Smirnov test of normality). The mean and median of the normalized prediction distribution error (NPDE) metrics for YSNSG in the plasma of the plasma and CNS model (Fig. 5A to 5D) were not significantly different from 0 ($p = 0.46$, one sample t test; $p = 0.16$, Wilcoxon signed-rank test), and their distributions were not different from a normal distribution ($p = 0.09$, Kolmogorov-Smirnov test of normality). The mean and median of the normalized prediction distribution error (NPDE) metrics for YSNSG in the CNS of the

plasma and CNS models (Fig. 5E to 5H) were not significantly different from 0 ($p = 0.30$, One-sample t test; $p = 0.08$, Wilcoxon signed-rank test), and their distributions were not different from a normal distribution ($p = 0.07$, Kolmogorov-Smirnov test of normality).

As shown in Fig. 4 and Fig. 5, the IWRES vs. time and IWRES vs. predictions were centered around zero, without systematic bias, and most values were within ± 2 standard deviations (SDs) (about the 5^{th} and 95^{th} percentiles of a normal distribution). The prediction-corrected visual predictive check for YSNSG (plasma or SC concentration of plasma and SC model; plasma or CNS concentration of plasma and CNS model) showed that the 5^{th}, 50^{th} and 95^{th} percentiles of the observed data were within the 90 % confidence interval of the 5^{th}, 50^{th} and 95^{th} simulated percentiles, respectively (Fig. 2C and 2D; Fig. 3C and 3D). The observations were contained within the prediction intervals, and the models appeared appropriate to describe the observed data. Considering these above evaluations, the model performances appeared acceptable and could be used in the pharmacokinetic simulations.

3.5. Simulations based on the pharmacokinetic model

During preclinical *in vitro* studies, YSNSG was reported to inhibit UALL-903 melanoma cell proliferation by 29 % and 40 %, respectively, for 5.000 and 10.000 ng/mL ($p < 0.01$ versus control) (Thevenard et al., 2006). Based on these data and our validated pharmacokinetic models, we carried out predictions for both active concentrations of YSNSG (Fig. 6). For a constant-rate, continuous infusion of both peptide concentrations, four infusion rates were determined for SC and CNS tissues, respectively. For SC tissue, the infusion rates were 147.471 ng/min and 294.942 ng/min, respectively. For CNS tissue, the infusions rates were 472.415 ng/min and 944.830 ng/min, respectively, for the same concentrations target.

4. Discussion

As part of the development of a molecule with antitumor properties, we investigated, for the first time, its plasma and tissue pharmacokinetics. After a single intravenous administration,

we showed a bicompartmental plasmatic elimination. Preliminary experimentation has already hypothesized a similar profile with the unique IV administration of 45 mg/kg (data not shown). The global volume of distribution at a steady state (Vd_{ss}) from the central to peripheral compartments appears to be high (433.7 ± 272.2 mL) in male rats weighing 300 g for the non-compartmental approach, according to the mean blood volume of male Wistar rats (6.44 mL/100 g) (Lee and Blaufox, 1985). As determined, the plasma protein binding appears to be low, so we can hypothesize that YSNSG pharmacokinetics is probably not influenced by plasma protein binding and, consequently, not exposed to drug-drug interactions with other drugs that are strongly bound to plasma proteins.

YSNSG is not the first molecule targeting integrin alpha v beta 3 to be studied for its antitumor properties. ATN-161 and cilengitide, for example, were also investigated in preclinical studies and are currently under clinical studies against many tumors. ATN-161 is a five-amino-acid peptide (without the RGD sequence) that was previously demonstrated to have anti-invasive and anti-metastatic properties (Khalili et al., 2006; Livant et al., 2000; Stoeltzing et al., 2003). Pharmacokinetic data showed in mice that, for 10 mg/kg, an order half-life elimination was visually determined between 73 and 79 min (Doñate et al., 2008). In a phase 1 study with 26 subjects, 0.1 to 16.0 mg/kg ATN showed an order half-life elimination higher than preclinical data (between 192 and 300 min) and total receptor saturation for high concentrations (Cianfrocca et al., 2006). Cilengitide (cyclo(-RGDf[*N*Me]V-)) also targets $\alpha_v\beta_3$ and inhibits *in vivo* tumor growth as ATN-161 and YSNSG. Two preclinical studies each reported some plasma pharmacokinetic parameters after intraperitoneal intravenous injection. Mikkelsen *et al*. found the central and peripheral volumes of distribution to be 320.0 mL/kg and 28.8 mL/kg, respectively (Mikkelsen et al., 2009), and Dolgos *et al*. found a volume of distribution 340 mL/kg (Dolgos et al., 2016). While the central volume of distribution (V_c) of cilengitide appears to be similar to that of

YSNSG, the peripheral volume of distribution (V_p) of cilengitide is lower than that of YSNSG and indicates a significantly higher disposition of YSNSG from the central to peripheral compartments. Consequently, the half-life elimination values of cilengitide (1.2 h and 0.24-0.5 h) appear to be lower than those of YSNSG, and the total clearance values were higher (924 mL/h/kg and 980 mL/h/kg). In a phase 1 study with 37 subjects, dosages from 30 to 1600 mg/m² showed a half-life elimination of 3-5 h, findings similar to those previously described in preclinical studies (Eskens et al., 2003). Considering the pharmacokinetics preclinical and clinical data for both molecules, YSNSG administration in humans appears to be feasible in practice while taking into account species differences (Dolgos et al., 2016).

The tissue pharmacokinetic approach using YSNSG focused on two peripheral tissues, subcutaneous and cerebral tissue. The choice of subcutaneous tissue as a superficial tissue seems to be consistent with previous preclinical studies that demonstrate antitumor activity *in vivo* against cutaneous melanoma in mice (Thevenard et al., 2010, 2006). The choice of cerebral tissue was based on two hypotheses. First, it is known that integrin $\alpha_v\beta_3$ is well expressed in tumor cerebral tissue, whether primary (glioma) or secondary (cerebral metastasis from melanoma for example) (Kuphal et al., 2005; MacDonald et al., 2001; Schittenhelm et al., 2013). Second, cilengitide shows modest activity in glioblastoma (Nabors et al., 2015; Reardon et al., 2008; Stupp et al., 2014).

Microdialysis recovery using the reverse dialysis method without an internal standard indicated recovery rates consistent with the use of a perfusion rate of 1 µL/min and a semipermeable membrane of 4 mm (Chaurasia et al., 2007; Plock and Kloft, 2005). For both tissues, we identified and quantified YSNSG after a unique intravenous administration. In subcutaneous tissue, the pharmacokinetic profile appears to be similar to the plasmatic pharmacokinetic profile. C_{max} (9.53 ± 2.38 µg/mL) was achieved rapidly, and elimination appeared as a bicompartmental profile. The penetration rate of YSNSG from plasma to

subcutaneous tissue was 66.2 ±21.6 % (AUC ratios), a value that is consistent with a disposition from the central to superficial peripheral compartment. The concentrations of YSNSG appears to be compatible with the antitumor pharmacological activity (inhibition of cancer cell proliferation), according to the determined active concentrations (5.08-10.16 µg/mL) (Thevenard et al., 2006). Not surprisingly, the cerebral pharmacokinetic profile and concentrations of YSNSG differ from those of subcutaneous tissue. T_{max} was achieved between 60 and 90 minutes, probably due to BBB (Blood Brain Barrier) penetration. C_{max} was approximately fifty fold lower than the SC C_{max}. Consequently, the penetration rate from the central compartment to cerebral tissue was low (3.6 ± 4.7 %), and minimal antitumor pharmacological concentrations were not achieved. These data are consistent with the physiological function of the BBB as a functional protection barrier against exogenous molecules like drugs. Some therapeutic compounds entering development failed to achieve pharmacological concentrations in CNS due to the BBB, and the literature showed that only 7 % of drugs in development reach the marketplace (Kaitin, 2005). Moreover, this penetration rate may suggest that a 30-minute waiting period after cerebral probe implantation is sufficient to preserve the function of the BBB, as previously described (De Lange et al., 1995).

Our study has limitations. First, we used only one dosage (10 mg/kg) of YSNSG except for a preliminary experimentation with 45 mg/kg. Second, the number of rats was low but was in accordance with the ethics committee guidelines and microdialysis interest. Microdialysis is a good compromise in order to reduce the number of animals but can lead to an over-parameterized model and as a result the number of data necessary induces shrinkage. As shown in Table 2, the impact of shrinkage is important for V2 (63 and 62%, respectively, in subcutaneous and cerebral tissue), demonstrates good identifiability properties of the proposed model and appears acceptable. All other shrinkage values are within 26%.

Our results are promising. The main pharmacokinetics parameters of the plasma are consistent with human experimentation, in the same way as cilengitide and ATN-161 which were administered twice and three a week respectively in phase 1 studies without discontinuation (Cianfrocca et al., 2006; Eskens et al., 2003). Tissue pharmacokinetic parameters indicate strong distribution in superficial peripheral tissue like subcutaneous tissue with active pharmacological concentrations. Further studies are needed to investigate YSNSG peptide distribution in non-healthy tissue like the tumor environment, for example, in the mice using the previously used melanoma model (Thevenard et al., 2010, 2006). These investigations could highlight the influence of the tumor microenvironment on peptide pharmacokinetics. This might induce a resistance phenomenon, leading to lower tissue concentrations and, consequently, lower pharmacological efficacy (Trédan et al., 2007). By contrast, as previously shown with ATN-161, we hypothesized that tissue elimination might be lower due to durable interactions between YSNSG and its target $\alpha_v\beta_3$ (Doñate et al., 2008). In further studies, we will use microdialysis, which appears to be a well-suited method to investigate the tissue distribution of exogenous drugs in healthy tissue like subcutaneous tissue. This method can also be used in other peripheral compartments or organs corresponding to frequent secondary localizations of melanoma metastasis such as the liver (Davies and Lunte, 1995; Ståhle et al., 1991).

5. Conclusions

We conducted the first pharmacokinetic study of YSNSG, which is a promising member of the new therapeutic class of αvβ3 antagonists. For tissue pharmacokinetics, we used microdialysis, which is one of the most appropriate methods to investigate drug distribution in some tissues of interest. The penetration rate of YSNSG from the plasma to subcutaneous tissue appears to be compatible with its pharmacological activity, which does not seem to be

feasible for CNS tissue. We currently hypothesized that YSNSG nanoencapsulation would enhance its penetration rate through BBB and reach pharmacological active concentrations. With plasmatic and tissue pharmacokinetic parameters, we carried out a pharmacokinetic-based model to describe our pharmacokinetic population. Combining microdialysis and pharmacokinetic modeling appears to be a successful method to predict minimum doses to be administered. Further investigations are needed to characterize dose-effect of YSNSG to appreciate pharmacokinetic distribution in a tumor tissue and investigate other tissues, such as the lung or liver, which are also the most preferred locations of melanoma metastasis.

Acknowledgments

The authors would like to thank Matthieu Kaltenbach for his help and guidance during the non-compartmental pharmacokinetic analysis.

References

Brooks, P.C., Clark, R.A., Cheresh, D.A., 1994. Requirement of vascular integrin alpha v beta 3 for angiogenesis. Science 264, 569–571.

Chaurasia, C.S., Müller, M., Bashaw, E.D., Benfeldt, E., Bolinder, J., Bullock, R., et al., 2007. AAPS-FDA Workshop White Paper: Microdialysis Principles, Application and Regulatory Perspectives. Pharm. Res. 24, 1014–1025.

Cianfrocca, M.E., Kimmel, K.A., Gallo, J., Cardoso, T., Brown, M.M., Hudes, G., et al., 2006. Phase 1 trial of the antiangiogenic peptide ATN-161 (Ac-PHSCN-NH(2)), a beta integrin antagonist, in patients with solid tumours. Br. J. Cancer 94, 1621–1626.

Danen, E.H., Van Muijen, G.N., Ruiter, D.J., 1995. Role of integrins as signal transducing cell adhesion molecules in human cutaneous melanoma. Cancer Surv. 24, 43–65.

Davies, M.I., Lunte, C.E., 1995. Microdialysis sampling for hepatic metabolism studies. Impact of microdialysis probe design and implantation technique on liver tissue. Drug. Metab. Dispos. 23, 1072–1079.

De Lange, E.C., de Vries, J.D., Zurcher, C., Danhof, M., de Boer, A.G., Breimer, D.D., 1995. The use of intracerebral microdialysis for the determination of pharmacokinetic profiles of anticancer drugs in tumor-bearing rat brain. Pharm. Res. 12, 1924–1931.

Djerada, Z., Feliu, C., Tournois, C., Vautier, D., Binet, L., Robinet, A., et al., 2013. Validation of a fast method for quantitative analysis of elvitegravir, raltegravir, maraviroc, etravirine, tenofovir, boceprevir and 10 other antiretroviral agents in human plasma samples with a new UPLC-MS/MS technology. J. Pharm. Biomed. Anal. 86, 100–111.

Djerada, Z., Fournet-Fayard, A., Gozalo, C., Lelarge, C., Lamiable, D., Millart, H., et al., 2014. Population pharmacokinetics of nefopam in elderly, with or without renal impairment, and its link to treatment response. Br. J. Clin. Pharmacol. 77, 1027–1038.

Dolgos, H., Freisleben, A., Wimmer, E., Scheible, H., Krätzer, F., Yamagata, T., et al., 2016. In vitro and in vivo drug disposition of cilengitide in animals and human. Pharmacol. Res. Perspect. 4, e00217.

Doñate, F., Parry, G.C., Shaked, Y., Hensley, H., Guan, X., Beck, I., et al., 2008. Pharmacology of the novel antiangiogenic peptide ATN-161 (Ac-PHSCN-NH2): observation of a U-shaped dose-response curve in several preclinical models of angiogenesis and tumor growth. Clin. Cancer Res. Off. J. Am. Assoc. Cancer Res. 14, 2137–2144.

Edward, M., 1995. Integrins and other adhesion molecules involved in melanocytic tumor progression. Curr. Opin. Oncol. 7, 185–191.

Eskens, F.A.L., Dumez, H., Hoekstra, R., Perschl, A., Brindley, C., Böttcher, et al., 2003. Phase I and pharmacokinetic study of continuous twice weekly intravenous administration of Cilengitide (EMD 121974), a novel inhibitor of the integrins αvβ3 and αvβ5 in patients with advanced solid tumours. Eur. J. Cancer 39, 917–926.

Felding-Habermann, B., Cheresh, D.A., 1993. Vitronectin and its receptors. Curr. Opin. Cell. Biol. 5, 864–868.

Francavilla, C., Maddaluno, L., Cavallaro, U., 2009. The functional role of cell adhesion molecules in tumor angiogenesis. Semin. Cancer Biol. 19, 298–309.

He, Y., Jiang, Y., Li, Y.-J., Liu, X.-H., Zhang, L., Liu, L.-J., et al., 2010. 19-peptide, a fragment of tumstatin, inhibits the growth of poorly differentiated gastric carcinoma cells in vitro and in vivo. J. Gastroenterol. Hepatol. 25, 935–941.

Hynes, R.O., 2002. Integrins: Bidirectional, Allosteric Signaling Machines. Cell 110, 673–687.

Kaitin K.I., 2005. Longer clinical times are extending time to market for new drugs in U.S. Tufts Center for the Study of Drug Development Impact Report. Nov/Dec;7(6). URL: http://csdd.tufts.edu/news/complete_story/pr_ir_nov_dec_ir (accessed 14 june, 2016).

Khalili, P., Arakelian, A., Chen, G., Plunkett, M.L., Beck, I., Parry, G.C., et al., 2006. A non-RGD-based integrin binding peptide (ATN-161) blocks breast cancer growth and metastasis in vivo. Mol. Cancer Ther. 5, 2271–2280.

Kim, K.B., Prieto, V., Joseph, R.W., Diwan, A.H., Gallick, G.E., Papadopoulos, N.E., et al., 2012. A randomized phase II study of cilengitide (EMD 121974) in patients with metastatic melanoma. Melanoma Res. 22, 294–301.

Kuphal, S., Bauer, R., Bosserhoff, A.-K., 2005. Integrin signaling in malignant melanoma. Cancer Metastasis Rev. 24, 195–222.

Lavielle, M., Ribba, B., 2016. Enhanced Method for Diagnosing Pharmacometric Models: Random Sampling from Conditional Distributions. Pharm. Res. 33, 2979-2988

Lee, H.B., Blaufox, M.D., 1985. Blood volume in the rat. J. Nucl. Med. Off. Publ. Soc. Nucl. Med. 26, 72–76.

Ley, K., Rivera-Nieves, J., Sandborn, W.J., Shattil, S., 2016. Integrin-based therapeutics: biological basis, clinical use and new drugs. Nat. Rev. Drug Discov. 15, 173–183. doi:10.1038/nrd.2015.10

Li, Y., Sun, L., He, Y., Liu, X., Liu, M., Wang, Q., et al., 2009. The anti-tumor properties of two tumstatin peptide fragments in human gastric carcinoma. Acta Pharmacol. Sin. 30, 1307–1315.

Livant, D.L., Brabec, R.K., Pienta, K.J., Allen, D.L., Kurachi, K., Markwart, S., et al., 2000. Anti-invasive, antitumorigenic, and antimetastatic activities of the PHSCN sequence in prostate carcinoma. Cancer Res. 60, 309–320.

MacDonald, T.J., Taga, T., Shimada, H., Tabrizi, P., Zlokovic, B.V., Cheresh, D.A., et al., 2001. Preferential susceptibility of brain tumors to the antiangiogenic effects of an alpha(v) integrin antagonist. Neurosurgery 48, 151–157.

Mikkelsen, T., Brodie, C., Finniss, S., Berens, M.E., Rennert, J.L., Nelson, K., et al., 2009. Radiation sensitization of glioblastoma by cilengitide has unanticipated schedule-dependency. Int. J. Cancer 124, 2719–2727.

Nabors, L.B., Fink, K.L., Mikkelsen, T., Grujicic, D., Tarnawski, R., Nam, D.H., et al., 2015. Two cilengitide regimens in combination with standard treatment for patients with newly diagnosed glioblastoma and unmethylated MGMT gene promoter: results of the open-label, controlled, randomized phase II CORE study. Neuro-Oncol. 17, 708–717.

Pierschbacher, M.D., Ruoslahti, E., 1984. Cell attachment activity of fibronectin can be duplicated by small synthetic fragments of the molecule. Nature 309, 30–33.

Plock, N., Kloft, C., 2005. Microdialysis—theoretical background and recent implementation in applied life-sciences. Eur. J. Pharm. Sci. 25, 1–24.

Reardon, D.A., Fink, K.L., Mikkelsen, T., Cloughesy, T.F., O'Neill, A., Plotkin, S., et al., 2008. Randomized phase II study of cilengitide, an integrin-targeting arginine-glycine-aspartic acid peptide, in recurrent glioblastoma multiforme. J. Clin. Oncol. 26, 5610–5617.

Scheller, D., Kolb, J., 1991. The internal reference technique in microdialysis: A practical approach to monitoring dialysis efficiency and to calculating tissue concentration from dialysate samples. J. Neurosci. Methods 40, 31–38.

Schittenhelm, J., Schwab, E.I., Sperveslage, J., Tatagiba, M., Meyermann, R., Fend, F., et al., 2013. Longitudinal expression analysis of αv integrins in human gliomas reveals upregulation of integrin αvβ3 as a negative prognostic factor. J. Neuropathol. Exp. Neurol. 72, 194–210.

Shattil, S.J., Kim, C., Ginsberg, M.H., 2010. The final steps of integrin activation: the end game. Nat. Rev. Mol. Cell Biol. 11, 288–300.

Soldi, R., Mitola, S., Strasly, M., Defilippi, P., Tarone, G., Bussolino, F., 1999. Role of αvβ3 integrin in the activation of vascular endothelial growth factor receptor-2. EMBO J. 18, 882–892.

Ståhle, L., Arner, P., Ungerstedt, U., 1991. Drug distribution studies with microdialysis. III: Extracellular concentration of caffeine in adipose tissue in man. Life Sci. 49, 1853–1858.

Stoeltzing, O., Liu, W., Reinmuth, N., Fan, F., Parry, G.C., Parikh, A.A., et al., 2003. Inhibition of integrin alpha5beta1 function with a small peptide (ATN-161) plus continuous 5-FU infusion reduces colorectal liver metastases and improves survival in mice. Int. J. Cancer 104, 496–503.

Stupp, R., Hegi, M.E., Gorlia, T., Erridge, S.C., Perry, J., Hong, Y.-K., et al., 2014. Cilengitide combined with standard treatment for patients with newly diagnosed

glioblastoma with methylated MGMT promoter (CENTRIC EORTC 26071-22072 study): a multicentre, randomised, open-label, phase 3 trial. Lancet Oncol. 15, 1100–1108.

Thevenard, J., Floquet, N., Ramont, L., Prost, E., Nuzillard, J.-M., Dauchez, M., et al., 2006. Structural and Antitumor Properties of the YSNSG Cyclopeptide Derived from Tumstatin. Chem. Biol. 13, 1307–1315.

Thevenard, J., Ramont, L., Devy, J., Brassart, B., Dupont-Deshorgue, A., Floquet, N., et al., 2010. The YSNSG cyclopeptide derived from tumstatin inhibits tumor angiogenesis by down-regulating endothelial cell migration. Int. J. Cancer 126, 1055–1066.

Trédan, O., Galmarini, C.M., Patel, K., Tannock, I.F., 2007. Drug resistance and the solid tumor microenvironment. J. Natl. Cancer Inst. 99, 1441–1454.

Vansteenkiste, J., Barlesi, F., Waller, C.F., Bennouna, J., Gridelli, C., Goekkurt, E., et al., 2015. Cilengitide combined with cetuximab and platinum-based chemotherapy as first-line treatment in advanced non-small-cell lung cancer (NSCLC) patients: results of an open-label, randomized, controlled phase II study (CERTO). Ann. Oncol. Off. J. Eur. Soc. Med. Oncol. ESMO 26, 1734–1740.

Vermorken, J.B., Peyrade, F., Krauss, J., Mesía, R., Remenar, E., Gauler, T.C., et al., 2014. Cisplatin, 5-fluorouracil, and cetuximab (PFE) with or without cilengitide in recurrent/metastatic squamous cell carcinoma of the head and neck: results of the randomized phase I/II ADVANTAGE trial (phase II part). Ann. Oncol. Off. J. Eur. Soc. Med. Oncol. ESMO 25, 682–688.

Ye, H., Yao, Y., Jiang, X., Yuan, X., 2013. Tumstatin transfected into human glioma cell line U251 represses tumor growth by inhibiting angiogenesis. Chin. Med. J. 126, 1720–1725.

List of Figures and Tables

Fig. 1: Schematic representation of structural pharmacokinetic models for peptide YSNSG. CL, clearance; Cmt, compartment; V: Volume of compartment; K: elimination constant; k13, k31, k12 and k12: transfer microconstants.

Fig. 2: Goodness-of-fit plots for the final population-based plasma-subcutaneous model. A) Observed (Obs) YSNSG plasma concentrations [ng/mL] vs. individual-predicted (Ind.pred) YSNSG concentrations [ng/mL] B) Observed (Obs) YSNSG subcutaneous concentrations [ng/mL] vs. individual-predicted (Ind.pred) YSNSG. Prediction-corrected visual predictive check (PC-VPC) based on 1000 simulated data sets for YSNSG plasma concentrations [ng/mL] (C) and for YSNSG subcutaneous concentration [ng/mL] over the time [min] (D). The green lines show the 5^{th}, 500^{th} and 95^{th} percentiles of observed data; the areas represent the 90% confidence interval around the simulated percentiles.

Fig. 3: Goodness-of-fit plots for the final population-based plasma-CNS model. A) Observed (Obs) YSNSG plasma concentrations [ng/mL] vs. individual-predicted (Ind.pred) YSNSG concentrations [ng/mL] B) Observed (Obs) YSNSG CNS concentrations [ng/mL] vs. individual-predicted (Ind.pred) YSNSG. Prediction-corrected visual predictive check (PC-VPC) based on 1000 simulated data sets for YSNSG plasma concentrations [ng/mL] (C) and for YSNSG CNS concentration [ng/mL] (D) over the time [min]. The green lines show the 5th, 500th and 95th percentiles of observed data; the areas represent the 90% confidence interval around the simulated percentiles.

Fig. 4: Diagnostic plots for YSNSG plasma subcutaneous model.

For YSNSG plasma concentration or y1 [: individual Weighted RESiduals (IWRES) vs. time [min] (A) and versus prediction y1 (B); Normalized Prediction Distribution Error (NPDE) as a function of time [min] (C) and as a function of population predicted y1 (D).

For YSNSG subcutaneous concentrations of YSNSG or y2: IWRES vs. time [min] (E) and versus prediction y1 (F); NPDE as a function of time [min] (G) and as a function of population predicted prediction y1 (H).

Fig. 5: Diagnostic plots for plasma CNS model.

For YSNSG plasma concentration or y1: individual Weighted RESiduals (IWRES) vs. time [min] (A) and versus prediction y1 (B); Normalized Prediction Distribution Error (NPDE) as a function of time [min] (C) and as a function of population predicted y1 (D).

For YSNSG CNS concentrations of YSNSG or y2: IWRES vs. time [min] (E) and versus prediction y1 (F); NPDE as a function of time [min] (G) and as a function of population predicted prediction y1 (H).

Fig. 6: Predictions for both active concentrations of YSNSG cyclopeptide with a fixed rate and continuous infusion in subcutaneous and CNS tissue. In order: prediction for active concentration of YSNSG cyclopeptide with a constant rate of 5,000 ng/mL in plasma (**A**) and subcutaneous tissue (**B**); prediction for active concentration of YSNSG cyclopeptide with a constant rate of 10,000 ng/mL in plasma (**C**) and subcutaneous tissue (**D**). Median values of simulated concentrations were performed using MlxPlore V.1 software (lixoft, France) and validated population pharmacokinetic model. *This graphical image has been built from MlxPlore v.1 to enhance clarity without deliberate wish to manipulate their interpretation*

Fig. 6 (continuum): Predictions for both active concentrations of YSNSG cyclopeptide with a fixed rate and continuous infusion in subcutaneous and CNS tissue. In order: prediction for

active concentration of YSNSG cyclopeptide with a constant rate of 5,000 ng/mL in plasma (**E**) and cerebral tissue (**F**); prediction for active concentration of YSNSG cyclopeptide with a constant rate of 10,000 ng/mL in plasma (**G**) and cerebral tissue (**H**). Median values of simulated concentrations were performed using MlxPlore V.1 software (lixoft, France) and validated population pharmacokinetic model. *This graphical image has been built from MlxPlore v.1 to enhance clarity without deliberate wish to manipulate their interpretation*

610 **Table 1:** Individual plasma and tissue parameters of peptide YSNSG after a single injection
611 (10 mg/kg) on Wistar rat (n=12).

612 **Table 2:** Parameter Estimates of the final YSNSG peptide population-based pharmacokinetic
613 Model.

614

615

616

617 Table 1: Plasma and tissue pharmacokinetic of peptide YSNSG in Wistar Rats (n=12)

Pharmacokinetic parameters	**Mean±S.D.**	**R.S.E (%)**
Plasma pharmacokinetic parameters		
Dose of peptide YSNSG (µg)	3073±134	1
A (µg)	16.581±4.957	7
α (min^{-1})	0.08694±0.06723	21
$t_{1/2}\alpha$ (min)	12.7±6.9	9
B (µg)	4.61±4.23	21
β (min^{-1})	0.00678±0.00479	12
$t_{1/2}\beta$ (min)	154.0±91.0	10
Vc (mL)	158.3±52.1	6
Vp (mL)	275.4±243.3	18
Vdss (mL)	433.7±272.2	13
k_{21}	0.0288±0.0304	27
k_{10}	0.0251±0.010	10
k_{12}	0.0398±0.0412	27
Cl (mL/min)	3.8±1.6	14
AUC_p (µg/min/mL)	1059.94±744,42	14
Subcutaneous pharmacokinetic parameters		
C_{max} (µg/mL)	8.57±2.13	5
t_{max} interval (min)	0-30	-
AUC (µg/min/mL)	885.172±508.149	11
CNS pharmacokinetic parameters		
C_{max} (ng/mL)	183.4±200.4	22
T_{max} interval (min)	60-90	-
AUC (µg.min/mL)	24.22±20.97	17
Plasma – SC and Plasma/CNS AUC ratio		
AUC_{sc}/AUC_p ratio (%)	66.2±21.6	-
AUC_{cns}/AUC_p ratio (%)	3.6 ±4.7	-

SD: Standard Deviation; R.S.E.: Relative Standard Error; A: B: α: β: Vc: Volume of distribution for central compartment; Vp: Volume of distribution for peripheral compartment; Vd: volume of distribution; k21, K10 and k12: microtransfert constants; Cl: Total clearance; Cmax: Peak concentration; Tmax: Time to reach Cmax; SC: Subcutaneous; CNS: Central Nervous System

Table 2: Parameter Estimates of the final YSNSG peptide physiologically-based pharmacokinetic Model

Pharmacokinetic population parameters	**Mean (R.S.E, %) and shrinkage values**			
Parameter	**Plasma - subcutaneous model**	**Shrinkage**	**Plasma - CNS model**	**Shrinkage**
K	0.579 (10)	19%	0.669 (8)	8%
V1 (mL)	3.18 (6)	5%	3.27 (6)	21%
K12	0.262 (16)	2%	0.916 (3)	-12%
K21	0.00227 (33)	-1%	0.0302 (7)	-11%
K13	0.813 (8)	3%	0.00919 (13)	26%
K31	0.0535 (5)	-1%	NA[a]	NA[a]
V2 (mL)	97.6 (13)	63%	271 (51)	62%
Omega_k	0.309 (23)		0.262 (22)	
Omega_v1	0.0934 (74)		0.0834 (11.7)	
Omega_k12	0.506 (25)		0.0948 (22)	
Omega_k21	1.01 (24)		0.158 (43)	
Omega_k13	0.263 (21)		0.0814 (37.3)	
Omega_k31	0.0844 (70)		NA[a]	
Omega_v2	0.22 (51)		1.13 (32)	
B_1	0.543 (51)		0.519 (58)	
C_1	0.91 (7)		0.974 (7)	
B_2	0.218 (54)		0.269 (54)	
C_2	1.06 (7)		1.13 (11)	

Abbreviations: R.S.E.: Relative Standard Error ; CNS: Central Nervous System

[a] For both k31 = k13 and omega_k31 = omega_k13

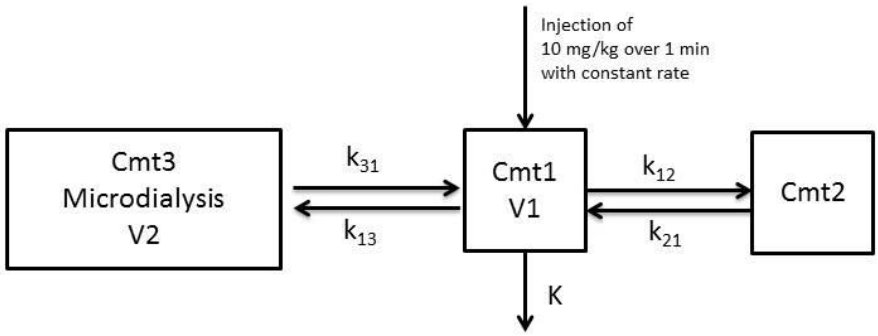

627

628

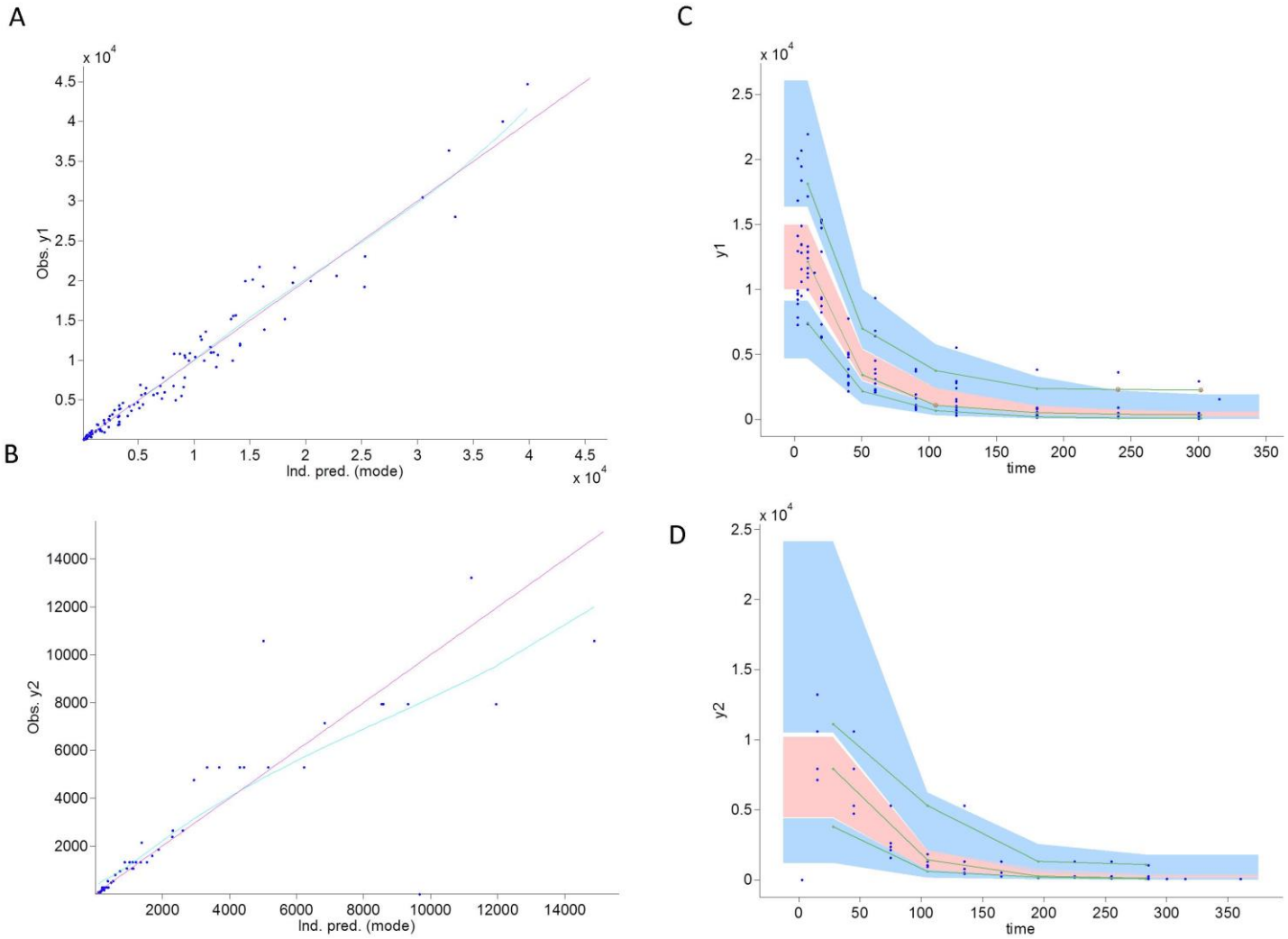
A
x 10^4
Obs. y1
Ind. pred. (mode)
x 10^4
B
Obs. y2
Ind. pred. (mode)
C
x 10^4
y1
time
D
x 10^4
y2
time

629

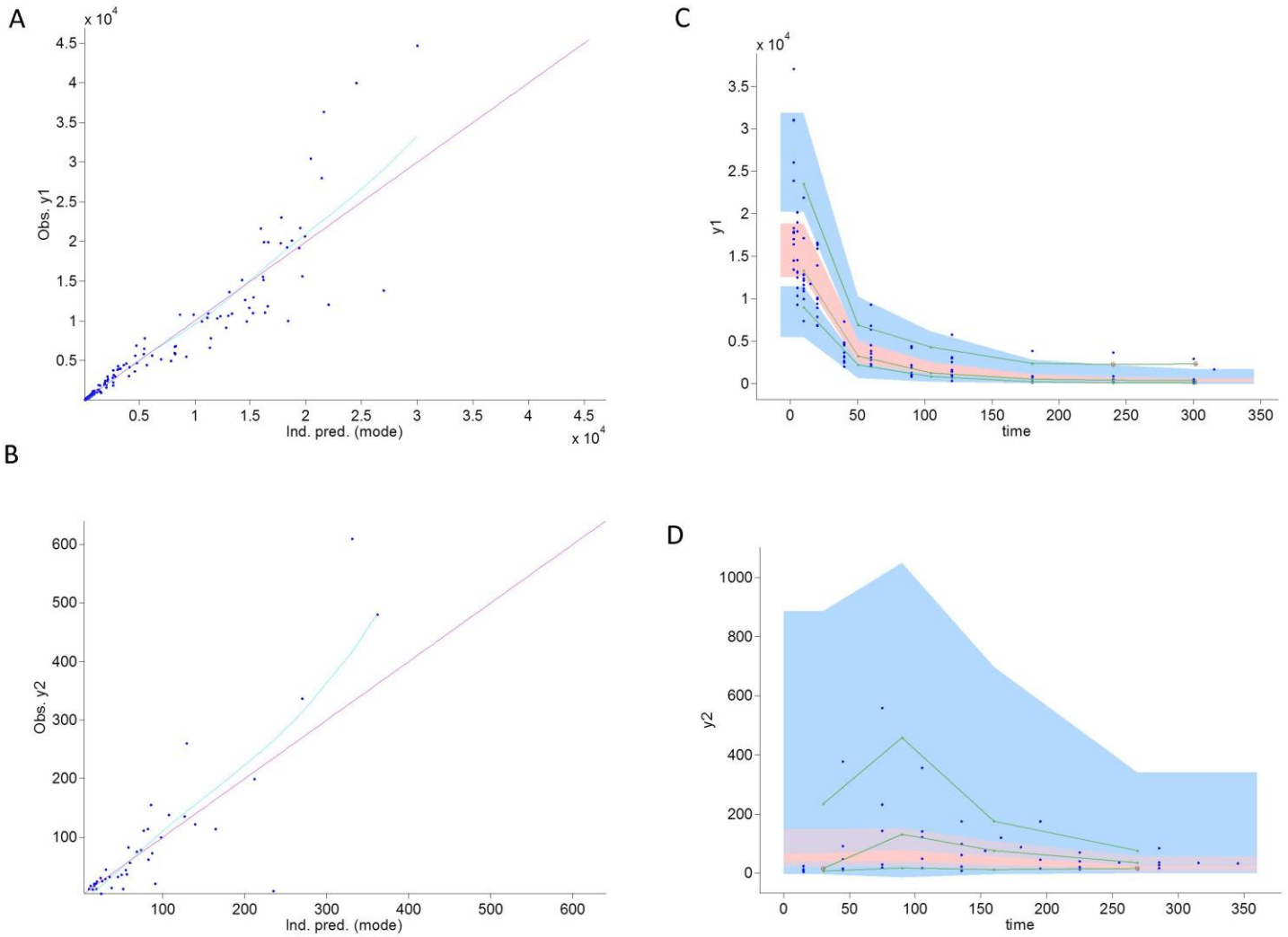
A
x 10^4
Obs. y1
Ind. pred. (mode)
x 10^4
B
Obs. y2
Ind. pred. (mode)
C
x 10^4
y1
time
D
y2
time

630

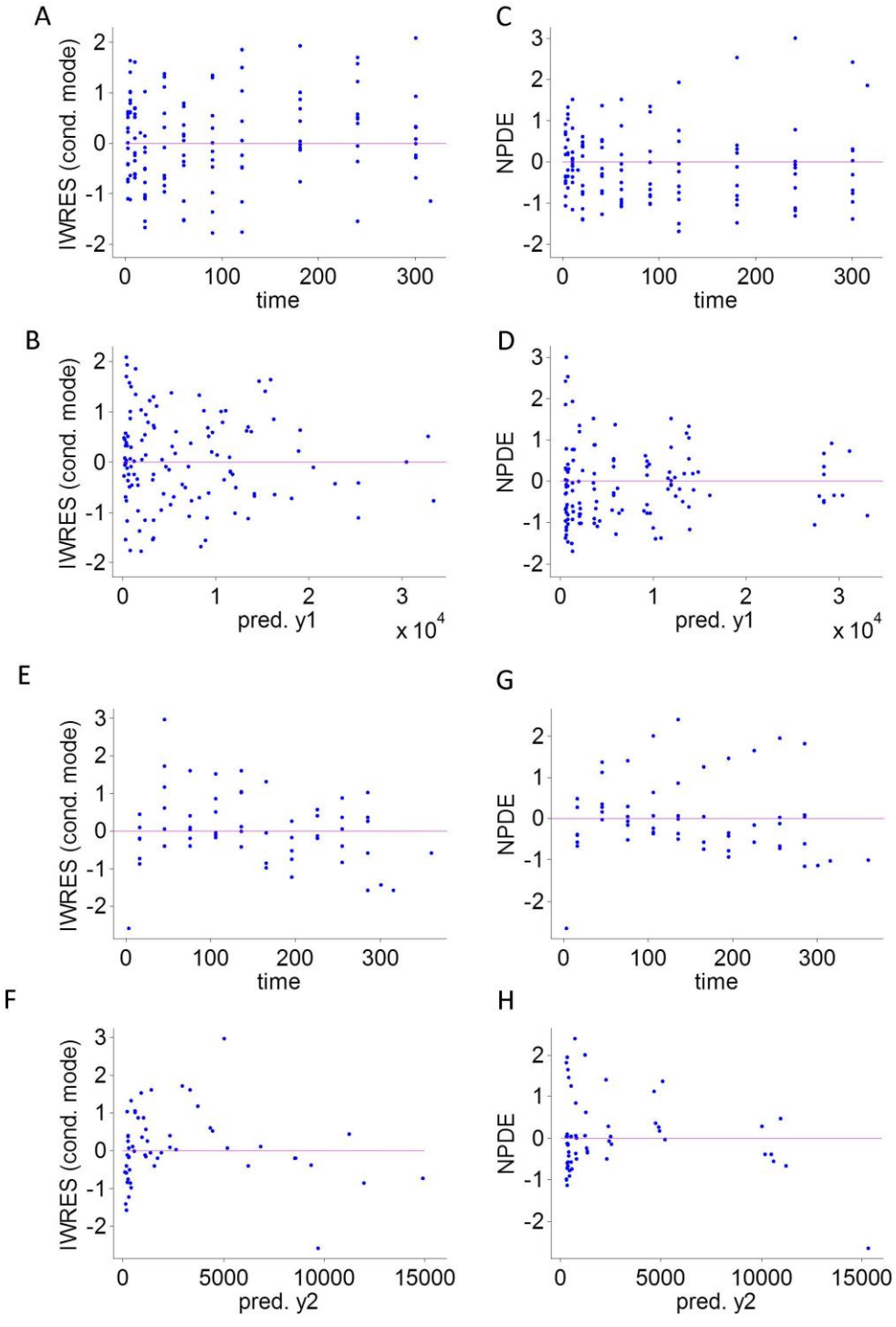
A
IWRES (cond. mode)
time
C
NPDE
time
B
IWRES (cond. mode)
pred. y1
x 10^4
D
NPDE
pred. y1
x 10^4
E
IWRES (cond. mode)
time
G
NPDE
time
F
IWRES (cond. mode)
pred. y2
H
NPDE
pred. y2

631

632

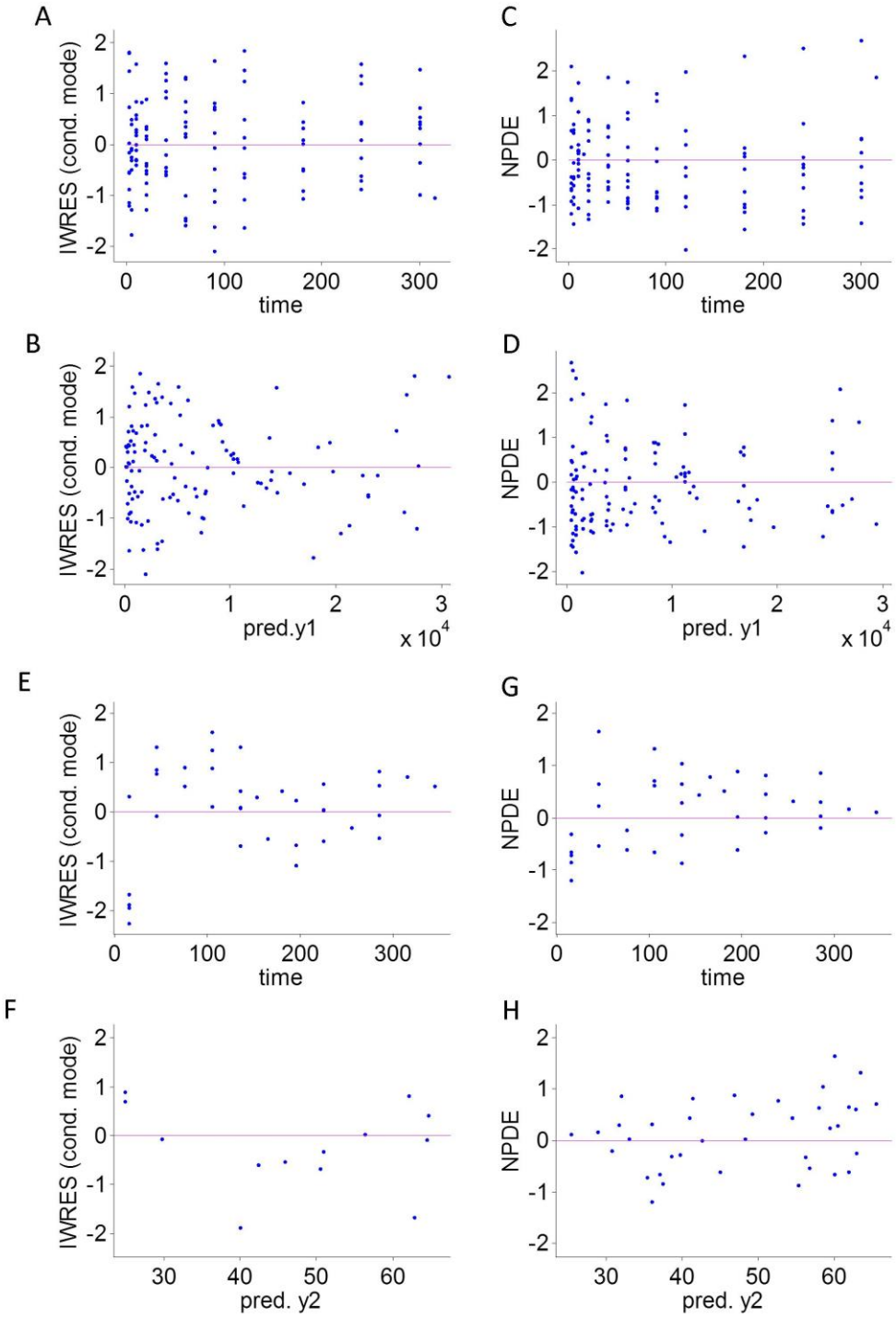
A
IWRES (cond. mode)
time
C
NPDE
time
B
IWRES (cond. mode)
pred.y1
x 10^4
D
NPDE
pred. y1
x 10^4
E
IWRES (cond. mode)
time
G
NPDE
time
F
IWRES (cond. mode)
pred. y2
H
NPDE
pred. y2

633

634

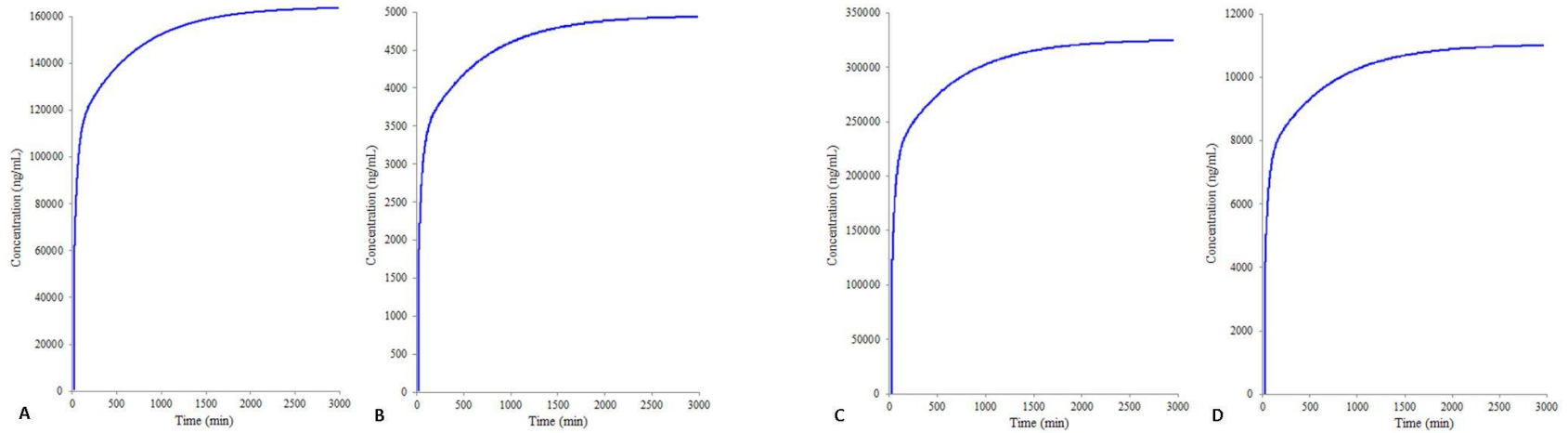
A
Concentration (ng/mL)
Time (min)
B
Concentration (ng/mL)
Time (min)
C
Concentration (ng/mL)
Time (min)
D
Concentration (ng/mL)
Time (min)

635

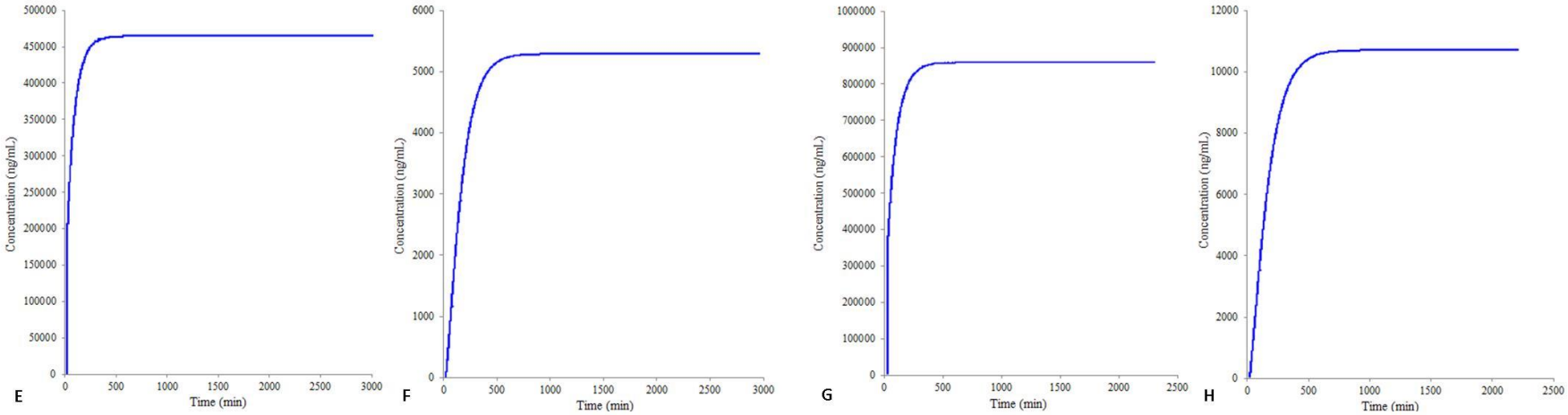
E
Concentration (ng/mL)
Time (min)
F
Concentration (ng/mL)
Time (min)
G
Concentration (ng/mL)
Time (min)
H
Concentration (ng/mL)
Time (min)

636